Catalysis Today 145 (2009) 288–293

Contents lists available at ScienceDirect

Catalysis Today

journal homepage: www.elsevier.com/locate/cattod

Dynamic "operando" observation of 1 wt% Pd-based TWCs: Simultaneous XAS/DRIFTS/mass spectrometry analysis of the effects of $Ce_{0.5}Zr_{0.5}O_2$ loading on structure, reactivity and performance

Anna Kubacka [a], Arturo Martínez-Arias [a], Marcos Fernández-García [a,*], Mark A. Newton [b,**]

[a] Instituto de Catálisis y Petroleoquímica, CSIC, C/Marie Curie 2, 28049 Madrid, Spain
[b] The European Synchrotron Radiation Facility, 6 Rue Jules Horowitz, BP-220, Grenoble, France

ARTICLE INFO

Article history:
Available online 13 November 2008

Keywords:
Pd-based TWCs
CeO_2–ZrO_2
Al_2O_3
Operando and in situ measurements
XANES
Energy dispersive EXAFS
DRIFTS
Mass spectrometry

ABSTRACT

The behavior of 1 wt% Pd-TWCs (three-way catalysts), containing up to 33 wt% $Ce_{0.5}Zr_{0.5}O_2$ is followed under reducing (CO) and oxidizing (NO) cycling conditions. The dynamic behavior of these systems is analyzed using a synchronous, time-resolved energy dispersive X-ray absorption spectroscopy (XAS), diffuse reflectance infrared Fourier transform spectroscopy (DRIFTS) and mass spectrometry (MS) set-up with subsecond time resolution. Two main physico-chemical phenomena corresponding to noble metal morphological (size/shape) changes and the redox behavior of the noble metal–promoter interface are shown to control the TWC response to NO/CO cycling conditions. Metal-only aspects strongly influence N–O dissociation and N–N coupling steps while the metal–promoter interface has a global influence on both N_2 and CO_2 formation via oxygen handling (storage/release) properties. The relative importance of these two phenomena is studied as a function of the $Ce_{0.5}Zr_{0.5}O_2$ promoter content of the catalysts.

1. Introduction

Three-way catalysts (TWC) are widely used to diminish pollutant emissions from gasoline engine powered vehicles [1]. Classical components of these systems usually include Rh, Pt, and/or Pd as active metals, ceria as promoter, and high surface alumina as the support [1,2]. In modern TWC formulations, the promotion by ceria has been extended to other structurally related oxide systems in order to increase or maintain the durability of the TWC while enhancing the oxygen storage capacity (OSC) properties of the catalyst [1–3]. In this sense, Ce–Zr mixed oxide systems, and most specially in alumina supported Ce–Zr mixed oxide configurations, have been considered as optimum metal supports as they provide greater OSC after thermal sintering, potentially increasing the useful lifetime of the catalytic system [3]. Concerning the active metal, the use of Pd as the only active metal component in TWC has received considerable attention. Part of this interest has been purely economic, resulting from the high cost and scarcity of Rh. However the availability of cleaner fuels, which ameliorates problems due to the sensitivity of Pd to sulphur poisoning, along with the remarkable intrinsic activity palladium has for oxidation reactions [1,2,4] have provided more fundamental catalytic drivers. Metal (Pd) and promoter (Ce–Zr) characteristics have been extensively studied under light-off or isothermal conditions but much less is known for cycling conditions, typical of TWC operation, in which the stoichiometry of the gas atmosphere (the oxidant to reducing molecule balance) oscillates around the stoichiometric point with a frequency of ca. 1–3 Hz [1–3].

Dispersive XAS provides a window into the structural and electronic properties of components within working catalysts on subsecond time scales [5–13]. In addition, a number of approaches that fuse structurally direct techniques, such as EXAFS and small/wide angle scattering SAXS/WAXS, with other spectroscopies such as Raman [14–16] and infrared [10,11,13,17] have been demonstrated. A suitable combination to partner bulk sensitive and time-resolving XAS technique is with a surface-sensitive spectroscopy such as infrared, as this can identify the molecular nature of adsorbed species and be used with a similar time-resolving power [10,11,13,17]. Previous studies have investigated aspects of either the catalytic [7,18,19] or the structural [8,9,13] behavior of Pd-TWCs

* Corresponding author. Tel.: +34 915854939; fax: +34 915854760.
** Corresponding author.
E-mail addresses: mfg@icp.csic.es (M. Fernández-García), newton@esrf.fr (M.A. Newton).

0920-5861/$ – see front matter © 2008 Elsevier B.V. All rights reserved.
doi:10.1016/j.cattod.2008.09.029

solids under oscillatory (lambda/cycling) conditions. While considerable detail regarding the Pd-TWC systems has been gleaned from these studies, the majority have involved conducting the spectroscopy/characterization and the reaction studies separately or through examining one aspect without the other. Here we utilize an approach that permits simultaneous, and internally self-consistent, investigation of three aspects of a working catalytic system: the structure/chemistry of the Pd component; the IR visible surface species present on the surface of the catalysts; and the overall catalytic activity/selectivity. As a result, we aim to maximize both the information that arises from a single experiment, and realize a more complete and reliable picture of some of the fundamental behavior that these catalysts display on timescales approaching those of relevance to the real lambda cycling situation.

In this paper we study two 1 wt% Pd-based TWC systems having a different loading of the Ce–Zr promoter. An increasing promoter loading would increase the metal–promoter interface (per gram of catalyst) and help in probing the role of such interface in the pollutant elimination chemistry. These catalysts have been fully characterized elsewhere [20,21]. We will show that the dynamic catalytic response of the systems during CO/NO cycling are radically different in many ways, and, further, illustrate the interplay between these two components in Pd-based Ce–Zr-promoted catalysts under cycling conditions. The main aim is to start toward fully characterizing the dynamical aspects of the catalytic behavior of the Pd-based TWC as a function of the metal–promoter interaction in order to understand basic physico-chemical phenomena occurring in time intervals about and below the second.

2. Experimental

The 1 wt% Pd on a 10 wt% or 33 wt% ceria–zirconia on alumina (1Pd1ZCA; 1Pd3ZCA samples, respectively) samples were synthesized as described previously [20,21]. Ceria–zirconia with 10 or 33 wt% of Ce–Zr mixed oxide content (expressed, in accordance with ICP-AES analysis, as $Ce_{0.5}Zr_{0.5}O_2$) on alumina (γ-Al_2O_3 Condea Puralox; S_{BET} 180 $m^2\ g^{-1}$) were used as supports (1ZCA and 3ZCA samples, respectively). The Ce–Zr containing materials were prepared by equimolar cerium–zirconium coprecipitation within reverse microemulsions followed by separation of the solid, rinsing with methanol, drying overnight at 393 K and calcination under air at 773 K for 2 h. S_{BET} values of 196 and 201 $m^2\ g^{-1}$ were obtained for 1ZCA and 3ZCA, respectively. The supports were impregnated (incipient wetness method) with aqueous solutions of Pd(II) nitrate (in order to achieve a 1 wt% loading in the final catalysts). These were then dried overnight at 393 K and subsequently calcined in air at 773 K for 2 h. No appreciable differences in S_{BET} values with respect to those of the supports were observed upon incorporation of the metals.

The experimental set-up used is a development of that initially demonstrated in studies of Rh-based catalysts [10,11,17]. ca. 40–50 mg of sample, sieved to a 80–110 μm fraction, are used per experiment. Experiments were carried out on beamline ID24 at the European Synchrotron Radiation Facility (ESRF). Energy dispersive XAS measurements utilized a Si (3 1 1) polychromator in Bragg configuration and a 16 bit FReLoN detector [22]. Methodologies for optimizing the X-ray beam and sample presentation [23] for obtaining dispersive EXAFS data for these samples were also implemented. DRIFTS measurements utilized a Bruker IFS 66 spectrometer, and a high sensitivity MCT detector. Samples were heated under a flow of He to 673 K and then subjected to cycles comprising alternate (CO first) flows (75 ml min^{-1}) of 5% CO/He (13.8 s) and 5% NO/He (13.8 s) while XAS, DRIFTS and MS data were collected synchronously. After finishing the cycle with an exposure to NO the flow is returned to a He flow and the experiment repeated at 673 K. The samples were then cooled under He to 300 K. The CO/NO cycling treatment allows completion of most of the noble metal physico-chemical phenomena triggered by the contact with the gas and, together with our time resolution (about 300 ms), yields a clearer picture of the phenomena that may be at work during such redox processes and how potentially important they may be during lambda cycling and overall catalytic operation within the paradigm of the TWC operation.

3. Results and discussion

The main m/z signals obtained by mass spectrometry (MS) during CO/NO switching at 673 K for the 1Pd1ZCA and 1Pd3ZCA samples, and 1ZCA and 3ZCA supports are reported in Fig. 1.

Fig. 1A displays m/z 28 and 30 profiles throughout the NO/CO switching. While m/z 28 contains two main contributions, CO from the gas inlet and N_2 formed as a product of the reaction, m/z 30 is mainly associated with NO as NO_2 is not present due to the lack of gas phase oxygen. The two contributions to the m/z 28 signal are self-evident in Fig. 1A during the NO part of the cycle where a strong initial decay is followed by a bump for the 3ZCA support and the two Pd-containing samples. Note that the initial decay of the

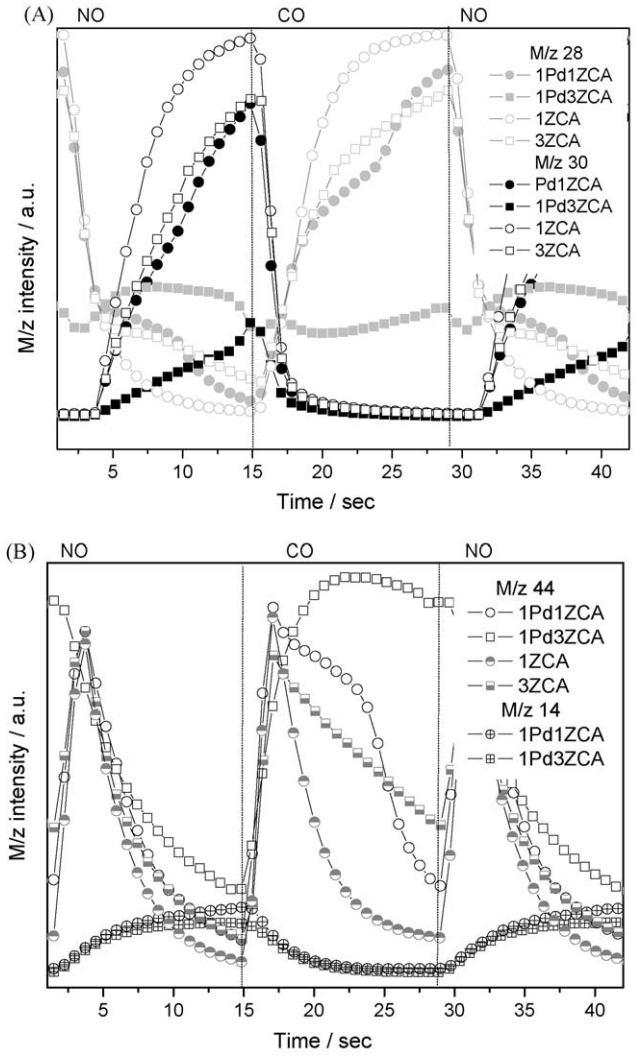

Fig. 1. Mass spectrometry signals during NO/CO (5% in He) cycling (75 ml min^{-1}) experiments at 673 K.

Pd3ZCA sample is different from the rest of the responses. The m/z 30 signal rises within this period but there is a clear consumption of NO for both the 1Pd1ZCA and 1Pd3ZCA catalysts in parallel to the N_2 formation. During the CO part of the treatment cycle, the m/z 28 consumption can be roughly estimated by the differences between the Pd-containing and support samples while the m/z 30 (NO) decay is rather similar for all systems.

To adequately analyze CO consumption we plot in Fig. 1B the m/z 44 signal (CO_2/N_2O). The comparison with the m/z 14 signal (nitrogen) behavior indicates that the 44 counterpart would essentially be associated with CO_2 formation. In addition we note that N_2O is not detected in the gas phase by DRIFTS (see below) during these experiments. CO_2 production is observed both during CO and NO steps of the cycling treatment. The CO_2 generated exclusively by the reducible Ce-containing promoter oxide is estimated (first approximation) using the bare supports. Concerning the Pd-containing systems we see that 1Pd1ZCA yields CO_2 in a limited amount in presence of NO gas and more easily in presence of CO gas. By contrast the 1Pd3ZCA catalyst produces significant amounts in both situations, in a way which significantly differs from the bare support and the other Pd-containing sample. In brief, Fig. 1 provides conclusive evidence that N_2, CO_2 production using 1Pd1ZCA is somehow connected with the properties of both the noble metal and promoter which need to work together to efficiently eliminate NO and CO. The 1Pd3ZCA system, however, shows a behavior that not easily interpreted as a simple sum of both components of the TWC and, as such provides evidence for a strong synergistic effect between the Pd nanoparticles and the ZCA support.

To further interpret such catalytic behavior, we present XAS/DRIFTS data collected in parallel with the mass spectrometric data during the NO/CO cycling treatment at 673 K. The Pd K-edge XANES spectrum of both catalysts suffers limited changes throughout the complete cycle and Fig. 2 shows representative examples under CO and NO gases. The edge position of both systems is indicative of a metallic state but the corresponding spectra display marked differences in the continuum resonances (CRs) position and intensity. The 1Pd1ZCA sample spectrum resembles the characteristic spectrum of a bulk metal with obvious differences in CR intensities due to particle size. Changes observed under CO and NO are exclusively due to size variations as justified using EXAFS (see below). The 1Pd3ZCA sample shows a strong valence d-electron deficiency (CR at ca. 24,355 eV), indicative of a d → sp rehybridization characteristic of very small cluster sizes, well below 10 atoms [24] and, most likely, significantly distorted away from a regular fcc structure (see for instance Huber et al. [25]). No apparent differences are in this case visible upon changes in gas phase nature.

By way of a more technical digression, whereas EXAFS data, and therefore formal EXAFS analysis, is possible for the 1Pd1ZCA sample (Fig. 2B and for instance, Ref. [13]), obtaining EXAFS (rather than XANES data) from the 1Pd3ZCA sample using this dispersive methodology still eludes us. One reason for this arises from the very small nature of the reduced Pd species. More importantly, however, this failure most likely has its source in the overall spatio-temporal stability of the X-ray beam/sample during experimentation, and the considerably increased small angle scattering effects that the 33 wt% $Ce_{0.5}Zr_{0.5}O_2$ domains will result in (as compared to that may result from the 10 wt% ZCA case). Such small angle scattering must be properly accounted for by the normalization measurement for reliable transmission energy dispersive EXAFS data. Whereas the normalization protocols (that have been introduced in an attempt to deal with this intrinsic weakness of the transmission-based dispersive experiment [23]) appear to be adequate in their ability to account for these effects at the 10 wt% ZCA level, they are still not satisfactory with higher loadings of the promoter and as such only XANES data is forthcoming in the 1Pd3ZCA case.

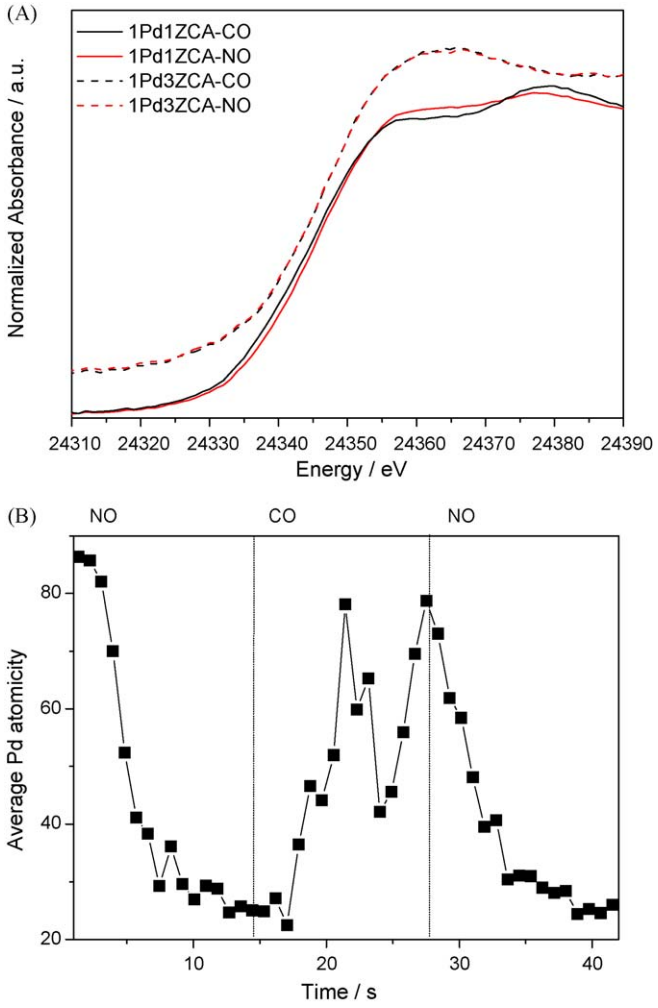

Fig. 2. (A) Representative XANES during NO/CO cycling experiments at 673 K and (B) EXAFS Pd average particle size during NO/CO cycling experiments at 673 K.

Estimation of the Pd particle size from EXAFS data in the case of 1Pd1ZCA was made following the method of Jentys [26]. The plot is also indicative of the 1Pd3ZCA size, which must be well below 30 atoms, in agreement with the size estimated based in the electronic information evolved from the XANES study. Interesting to note in Fig. 2B is the dynamical behavior of the Pd particle size/shape under NO/CO cycling which promotes reversible sintering/reshaping during reducing (CO) conditions and the corresponding redispersion/flattening under oxidizing (NO) conditions. This has been extensively analyzed in the 1Pd1ZCA case and the oxidation-less sintering/redispersion mechanism confirmed even in presence of gas phase oxygen [13,27]. Preliminary results indicate that this behavior is observed also in PdA and for ZCA-supported samples having promoter higher loadings than 10 wt%. The catalytic properties of 1Pd1ZCA under lambda oscillation seems to be intimately connected with this noble metal dynamical morphological cycle which may favor N atoms elimination from surfaces as the Pd particle grows and N–O dissociation as the particle present more unsaturated (edge, steps, and kinks) Pd surface entities [20,28–30]. Variations on the Pd–promoter interface also drive the corresponding interface oxygen activation and CO_2 production steps as detailed below [8,20]. More importantly, Fig. 2B provides

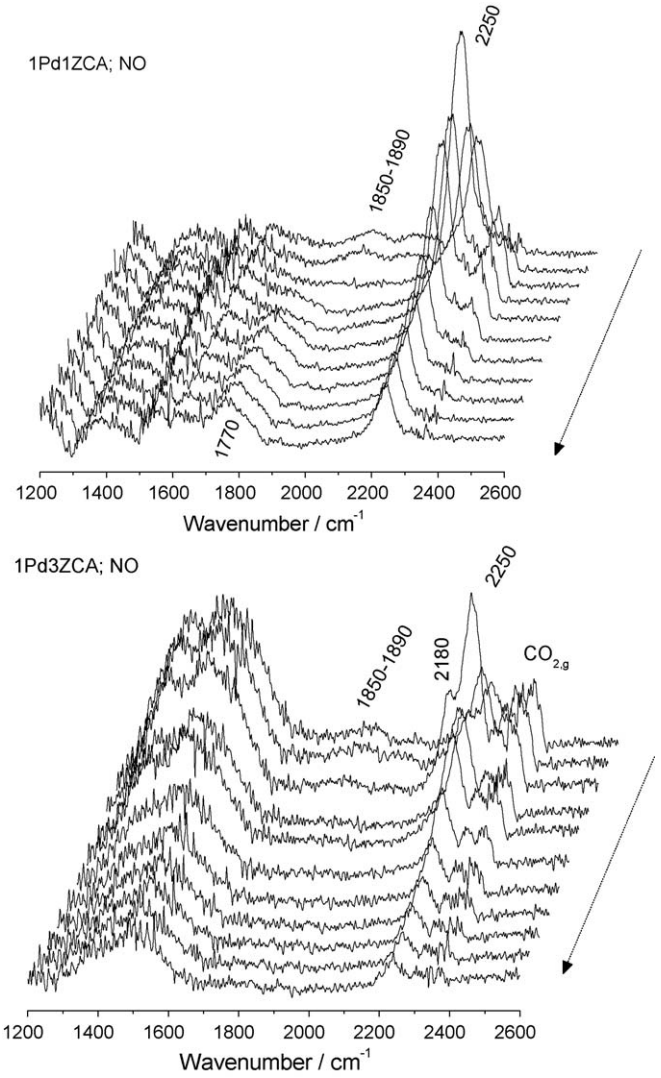

Fig. 3. Representative DRIFT spectra during the NO part of the cycling at 673 K. The arrow indicates increasing time after the switch in feed (to the gas indicated). Total temporal span—13.8 s.

evidence of the potential of these size/morphological changes to impact on catalyst behavior at the subsecond and second scale.

The synchronously acquired DRIFTS spectra from the 1Pd1ZCA and 1Pd3ZCA samples, respectively, are shown in Figs. 3 and 4. Fig. 3 plots the NO part of the cycle while Fig. 4 displays the CO counterpart. In "pseudo-stationary" conditions as shown in Fig. 1, both catalysts start the NO cycle with CO species (1850–1890 cm^{-1}) located at Pd bridge positions [13,20,21,28] and rising levels of NCO molecules (ca. 2250 cm^{-1}) adsorbed on alumina surfaces [13,31,32]. No N_2O gas signals (2210–2290; 1220–1265 cm^{-1}) are detected, indicating the high selectivity to N_2 within our experimental conditions. Pronounced differences between catalysts from an infrared perspective can be observed in the enhanced presence of carbonates (1300–1600 cm^{-1}) and CN (2180 cm^{-1}) species located at support sites of the 1Pd3ZCA sample, and of NO species (1770 cm^{-1}) by the middle-end part of the treatment in the 1Pd1ZCA case [13,20,21,33]. Note that CNO and CN species may be present at metal surfaces but at the working temperature such species are enough labile to be absent from our IR spectra [20,21]. CN species are likely formed by NCO decomposition on metal surfaces or, alternatively, by C–O dissociation, either directly or though the Boudouart reaction ($2CO \rightarrow C + CO_2$) [20,30,32].

During the CO step of the cycle (Fig. 4), we again detect the presence of Pd–CO and NCO for both Pd samples while differences among them are mainly related to CN/carbonates or Pd–NO species detected for, respectively, 1Pd3ZCA or 1Pd1ZCA systems. Carbonates apart (their overall intensity compared with CO_2(g) evolution suggests that most of them must be spectators, especially in the 1Pd3ZCA case), Fig. 5 illustrates the behavior of the principle IR observable adsorbate features and of the $CO_{2,g}$ contribution for both samples investigated. Figs. 3–5 are presented in absorbance units. As, in this case, our discussion is based on a qualitative analysis of intensity trends, the outcome is essentially independent of the units used. Indeed the recent work of Sirita et al. [34] has indicated that the use of absorbance instead of Kubelka–Munk units for small DRIFTS signals is qualitatively and quantitatively valid in such cases.

Firstly we may note the similitude between the CO_2 profiles detected with IR (Fig. 5) and MS (Fig. 1). Secondly we might note that, whereas Fig. 5 is indicative of CO adsorbing on Pd in both cases, no evidence for the formation of molecular NO species on Pd can be derived from the DRIFTS in the 1Pd3ZCA case, whereas the formation of such molecular NO species in the 1Pd1ZCA case during the NO cycle is quite clear.

The XAS/DRIFT/MS information allows us to interpret on physical a basis the differences in catalytic behavior between the two Pd-TWCs. Under NO, it can be seen that the 1Pd3ZCA

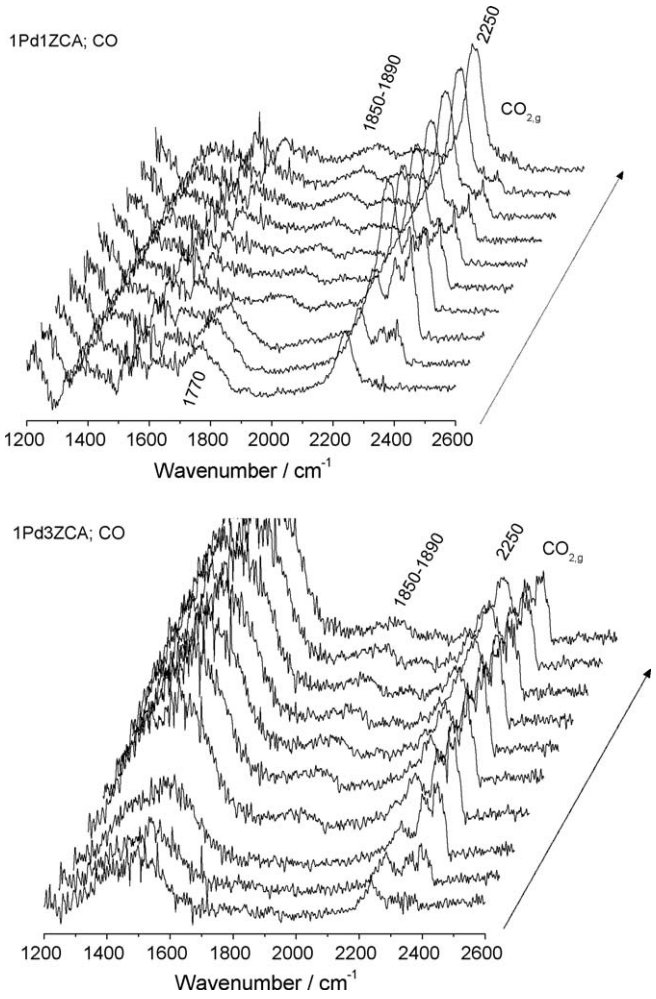

Fig. 4. Representative DRIFT spectra during the CO part of the cycling at 673 K. The arrow indicates increasing time after the switch in feed (to the gas indicated). Total temporal span—13.8 s.

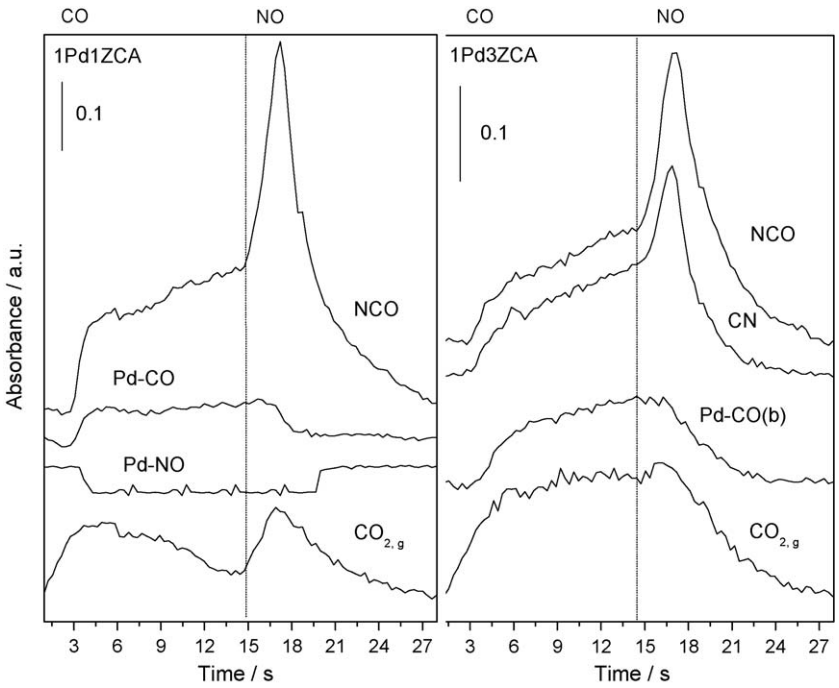

Fig. 5. DRIFTS peak intensity for selected species during NO/CO cycling experiments at 673 K.

system must dissociate NO more efficiently (Fig. 1), diminishing the molecular NO coverage with respect to 1Pd1ZCA (Fig. 3) and giving a significantly larger quantity of N_2 (Fig. 1). Although N–O dissociation may be favored in the case of 1Pd3ZCA vs. 1Pd1ZCA, a key point from a mechanistic point of view is the fact that the facility of N–N coupling decreases as the Pd primary particle size is diminished [28–30]. This indicates that metal-only aspects would favor the activity of the 1Pd1ZCA samples vs. the 1Pd3ZCA one for N_2 formation. Therefore, the capital role played by the Pd–promoter interface (including oxygen buffering effects) in 1Pd3ZCA becomes evident from the comparison of the two Pd-containing samples. Oxygen vacancies located in the immediate neighborhood of the very small Pd particles may limit the negative influence of the Pd particle size and overcome any other physical parameter influencing N_2 formation, "enhancing" the activity of the 1Pd1ZCA and 1Pd3ZCA samples in both N_2 and CO_2 formation [21,35]. Differences between catalysts in the handling of N-containing species are also related to the formation of CN species (2180 cm^{-1}; Figs. 3–5) but the location of such species at support sites makes any straightforward connection with previous mechanism steps difficult. Although the formation of this species is likely related to NCO evolution on Pd surfaces [32], its presence in the 1Pd3ZCA case may indicate more free Pd surface sites for N_2 evolution as well. This again connects with the promotion of oxygen and nitrogen activation through interface sites.

The behavior under CO and, generally speaking, the formation of CO_2 correspond to more complex phenomena. For 1Pd1ZCA, the Pd particle size/shape modification detected by EXAFS (Fig. 2B) has an obvious correlation with CO_2 production indicating parallel phenomena yet to be fully unraveled [13,27]; however, for the small 1Pd3ZCA noble metal particle we can see a behavior that results in an increasing formation of CO_2 up to an pseudo-stationary region through the middle-ending part of the CO step of the cycling (Fig. 5). The initial rising part is also paralleled by the increase in Pd–CO intensity, which is in turn related to the available Pd free sites by elimination of N-containing fragments. Assuming complete transference of the 1Pd1ZCA result, this would concomitantly occur with some Pd particle size growth but up to the levels above described (no appreciable EXAFS and particular XANES signals possibly indicating sizes well below 10–15 atoms). From a process perspective, the point to highlight is the ability of the 1Pd3ZCA sample to maintain a stable CO_2 production throughout the reducing (CO) cycle and into the initial seconds of the oxidising (NO) cycle. As XANES infers the absence of an oxygen source exclusively related with Pd, the enhanced CO_2 production seems a direct consequence of the Pd–promoter interface oxygen handling (storage/release) properties. A central issue for discussion in further works is, therefore, whether the Pd–promoter interface role differences among our samples can be rationalized as a function of differences in Pd particle size or are mostly related to other phenomena as the promoter oxygen lability as a function of the Ce–Zr size [20,21].

4. Concluding remarks

This work highlights that there are two main and inter-related phenomena occuring during redox (CO/NO) cycling, that can operate on time scales short enough to be able to control the catalytic performance of Pd-based TWCs. The first is related to Pd morphological (size/shape) dynamical changes occurring in a subsecond time scale [13,27]. In absence of significant oxidation of the noble metal, we detect Pd size/shape changes with may strongly influence in N_2 formation through a direct effect on N–O dissociation and N–N coupling steps. Due to the kinetic predominance of the N–N coupling step, this "metal-only" aspect would favor 1Pd1ZCA vs. 1Pd3ZCA for N_2 formation although results reported in Fig. 1 indicate the opposite situation. The detection of CN species suggests that O, N metallic surface coverage decreases for the 1Pd3ZCA case and may be a key point favoring activity. For 1Pd3ZCA, the underlying physical properties of the catalyst that dominate the observed catalytic behavior are not size/shape changes of a supported fcc Pd nanoparticle phase but are likely to result from a influence of the metal–promoter interface which results in exceptionally small Pd particles

intimately in contact with the CeZr phase. Thus, the second key aspect relates to the oxygen handling (storage/release) properties of the Pd–promoter interface, critical for the formation of both N_2 and CO_2 through specific details concerning both CO and NO molecules activation/dissociation [8,12].

Although the catalytic significance of the metal–promoter interface has been extensively studied in the past, the time-resolved results obtained using three (XAFS, DRIFTS, and MS) different and complementary probes simultaneously show that significant differences in oxygen handling (storage/release) properties between the 1Pd1ZCA and 1Pd3ZCA samples exist, and are directly linked to the overall behavior of the two systems. While the specifics of exactly how these effects arise require further study, the application of complementary time-resolved techniques, such as have been applied in the current case, show that a careful consideration of both noble metal and promoter particle size (along with and other morphological (shape) and surface characteristics) needs to be undertaken in order to fully explain the physical basis of the catalytic behavior of TWCs under lambda cycling conditions.

Acknowledgements

The authors acknowledge the CYCIT (projects CTQ2007-60480/BQU and CTQ2006-15600/BQU) for financial support of this job. Dr. A. Kubacka thanks the CSIC for a I3P postdoctoral grant. Dr. C. Belver is thanked for preparation of the samples used in this work. Gemma Guilera, Florian Perrin and Anna Kroner (ID24, ESRF) are also gratefully acknowleged for their technical and experimental support during the implementation of this experiment on ID24. The ESRF is thanking for provision of, and access to, the experimental facilities used in this work.

References

[1] E.S.J. Lox, B.H. Engler, in: G. Ertl, H. Knözinger, H.J. Weitkamp (Eds.), Environmental Catalysis, Wiley–VCH, 1999, p. 1.
[2] A. Martínez-Arias, J.C. Conesa, M. Fernández-García, J.A. Anderson, in: J.A. Anderson, M. Fernández-García (Eds.), Supported Metals in Catalysis, Imperial College Press, 2005, p. 283.
[3] J. Kašpar, P. Fornasiero, in: Trovarelli (Ed.), Catalysis by Ceria and Related Materials, Imperial College Press, 2002.
[4] R. van Yperen, D. Lindner, L. Mubmann, E.S. Lox, T. Kreuzer, Stud. Surf. Sci. Catal. 116 (1998) 51.
[5] M.A. Newton, A.J. Dent, J. Evans, Chem. Soc. Rev. 31 (2002) 83.
[6] A. Suzuki, Y. Inada, A. Yamaguchi, T. Chihara, M. Yuasa, M. Nomura, Y. Iwasawa, Angew. Chem. Int. Ed. 42 (2003) 4795.
[7] M.A. Newton, B. Jyoti, A.J. Dent, S.G. Fiddy, J. Evans, Chem. Commun. (2004) 2382.
[8] A. Iglesias-Juez, A. Martínez-Arias, M.A. Newton, S.G. Fiddy, M. Fernández-García, Chem. Commun. (2005) 4092.
[9] H. Tanaka, M. Uenishi, M. Taniguchi, I. Tan, K. Narita, M. Kimura, K. Kaneko, Y. Nishihata, J. Mizuki, Catal. Today 117 (2006) 321.
[10] M.A. Newton, A.J. Dent, S.G. Fiddy, B. Jyoti, J. Evans, Phys. Chem. Chem. Phys. 9 (2007) 246.
[11] M.A. Newton, A.J. Dent, S.G. Fiddy, B. Jyoti, J. Evans, Catal. Today 126 (64) (2007) 72.
[12] T. Yammamoto, A. Suzuki, Y. Nagai, T. Tanabe, F. Dong, Y. Inada, M. Nomura, Y. Iwasawa, Angew. Chem. Int. Ed. 46 (2007) 9253.
[13] M.A. Newton, C. Belver-Coldeira, A. Martínez-Arias, M. Fernández-García, Nat. Mater. 6 (2007) 528.
[14] A.M. Beale, Ad.M.J. van der Eerden, K. Kervinen, M.A. Newton, B.M. Weckhuysen, Chem. Commun. (2005) 3015.
[15] S.J. Tinnemans, J.G. Mesu, K. Kervinen, T. Visser, T.A. Nijhuis, A.M. Beale, D.E. Keller, Ad.M.J. van der Eerden, M.M. Weckhuysen, Catal. Today 113 (2006) 3.
[16] A.M. Beale, Ad.M.J. van der Eerden, S.D.M. Jacques, O. Leynaud, M.G. O'Brien, F. Meneau, S. Nikitenko, W. Bras, B.M. Weckhuysen, J. Am. Chem. Soc. 128 (2006) 12386.
[17] M.A. Newton, S.G. Fiddy, G. Guilera, B. Jyoti, J. Evans, Chem. Commun. (2005) 118.
[18] S. Wy, L. Xu, D. Weng, Appl. Surf. Sci. 221 (2004) 375.
[19] S.V. Christou, A.M. Efstathiou, Top. Catal. 42–43 (2007) 351.
[20] M. Fernández-García, A. Iglesias-Juez, A. Martínez-Arias, A.B. Hungría, J.A. Anderson, J.C. Conesa, J. Soria, Appl. Catal. B 31 (2001) 39.
[21] A. Iglesias-Juez, A. Martínez-Arias, M. Fernández-García, J. Catal. 221 (2004) 148.
[22] J.-C. Labiche, O. Mathon, S. Pascarelli, M.A. Newton, G. Guilera Ferre, C. Curfs, G. Vaughan, A. Homs, D. Fernandez Carreiras, Rev. Sci. Instrum. 78 (2007) 091301.
[23] M.A. Newton, J. Synchrotron Radiat. 14 (2007) 372.
[24] F. Illas, N. López, J.M. Ricart, A. Clotet, J.C. Conesa, M. Fernández-García, J. Phys. Chem. B 102 (1998) 8017.
[25] M.A. Hubert, et al. Nat. Mater. 5 (2006) 44.
[26] A. Jentys, Phys. Chem. Chem. Phys. 17 (1999) 4059.
[27] M.A. Newton, C. Belver-Coldeira, A. Martínez-Arias, M. Fernández-García, Angew. Chem. Int. Ed. 46 (2007) 8629.
[28] S.M. Vesecky, P. Chen, X. Xu, D.W. Goodmann, J. Vac. Sci. Technol. A 13 (1995) 1539.
[29] A.S. Worz, K. Juday, S. Abbeh, O. Heiz, J. Am. Chem. Soc. 125 (2003) 7964.
[30] J. Libuda, H.-J. Freund, Surf. Sci. Rep. 57 (2005) 157.
[31] M.L. Unland, J. Catal. 31 (1973) 469.
[32] F. Solymosi, T. Banasagi, J. Catal. 202 (2001) 205.
[33] S.A. Hendrick, S.S.C. Chuang, K. Almusaiteer Jr., R.W. Stevens, J. Phys. Chem. B 107 (2003) 4834.
[34] J. Sirita, S. Phanichphant, F.C. Meunier, Anal. Chem. 79 (2007) 3912.
[35] A. Martínez-Arias, J. Soria, J.C. Conesa, X.L. Seoane, A. Arcoya, R. Cataluña, J. Chem. Soc., Faraday Trans. 91 (1995) 1679.